ELSEVIER

Journal of Nuclear Materials 245 (1997) 224–237

journal of nuclear materials

Experimental study and modelling of copper precipitation under electron irradiation in dilute *Fe*Cu binary alloys

M.H. Mathon [1], A. Barbu *, F. Dunstetter, F. Maury, N. Lorenzelli, C.H. de Novion [2]

Laboratoire des Solides Irradiés, CEA-CEREM-DECM, Ecole Polytechnique, 91128 Palaiseau, France

Received 8 November 1996; accepted 10 December 1996

Abstract

In order to study the effect of the supersaturation of freely migrating defects on the precipitation of copper in high residual copper pressure vessel steels under neutron irradiation, *Fe*Cu (1.34, 0.30 and 0.11 at.% Cu) model alloys were irradiated between 175 and 360°C with high energy electrons. On-line electrical resistivity measurements and small angle neutron scattering (SANS) under magnetic field experiments were carried out. The use of the latter method to get the chemical composition of the precipitates is discussed. We show that the mechanisms of precipitation are identical under electron irradiation and under thermal aging. The sole effect of electron irradiation on the precipitation is to enhance the kinetics. A modelling of copper precipitation based on cluster dynamics is proposed. A comparison between our SANS results obtained under electron irradiation and those under neutron irradiation published in the literature shows that the mechanisms of precipitation are very likely different with both kinds of particles.

1. Introduction

It is well known that the irradiation hardening and related embrittlement of pressure vessel steels are very sensitive to the amount of residual copper. They are at least partially attributed to the precipitation of copper which has a very low solubility in iron. However, the mechanism of copper precipitation under irradiation is still now not correctly understood. This is the reason why we undertook a study of the unmixing in binary *Fe*Cu and ternary *Fe*CuM (M = Mn, Ni, Cr, P) model alloys under irradiation.

In this study, the irradiations are carried out with high energy electrons. The reason is that the actual irradiation, with neutrons, produces not only a supersaturation of point defects but also special effects in displacement cascades such as vacancy (and may be interstitial) clustering or even mixing. By choosing electron irradiations which create only isolated freely migrating point defects, it is possible to study separately one aspect: the effect of the point defect supersaturation. Then a comparison with neutron (or ion) irradiations should enable us to gain some information about the specific role of displacement cascades.

Study by electrical resistivity measurement of copper precipitation in $FeCu_{1.34\ at.\%}$, EXAFS in *Fe*Cu, *Fe*CuMn, *Fe*CuNi and some first results obtained by small angle neutron scattering on the same alloys have already been published [1–6].

This paper is a synthesis of previous and new results, about precipitation in binary *Fe*Cu alloys under electron irradiation.

2. Materials and techniques

2.1. Materials

The *Fe*Cu alloys containing 1.34, 0.30 and 0.11 at.% Cu were elaborated by the LETRAM/SRMA, CEA Saclay, from an iron containing: 0.2 at.% Al, 0.04 at.% Si, 0.012

* Corresponding author.

[1] Present address: Laboratoire Léon Brillouin (CEA-CNRS), 91191 Gif-sur-Yvette cedex, France.

[2] Present address: Laboratoire Léon Brillouin (CEA-CNRS), 91191 Gif-sur-Yvette cedex, France.

PII S0022-3115(97)00010-X

at.% S and 0.02 at.% P. As the vacancies migration energy E_1^m is known to be very sensitive to the carbon content around 10 apm (E_1^m varies from 0.6 eV for low C content to 1.3 eV for high C content), a carbon concentration of 100 apm was chosen. This value is not too low in order to get $E_1^m \cong 1.3$ eV as expected in steels and not too high in order to retain the simple ferritic structure.

The samples were cold-rolled and tiles of size $1.2 \times 3 \times 0.04$ cm^3 (for irradiation) or $1.5 \times 1.5 \times 0.08$ cm^3 (for thermal aging) were cut. They were annealed for 24 h at 820°C and quenched at $\cong$ 10°C/s.

2.2. Thermal aging

Some of the samples were thermally aged at 500°C for durations ranging from 2.5 h to 312 h, At this temperature, the precipitation is known to be homogeneous and the incubation time to be short [7,8].

2.3. Electron irradiations

The irradiations were carried out with 2.5 MeV electrons in a Van de Graaff accelerator at doses up to 5 C cm^{-2} (3.1×10^{19} e$^-$/cm^2, i.e., 1.4×10^{-3} dpa using a cross-section for point defects production of 50 barns). The dose rate was around 6×10^{-6} C cm^{-1} s^{-1} (4×10^{13} e$^-$ cm^{-2} s^{-1}, i.e., 2×10^{-9} dpa s^{-1}). The samples were only heated by the 20 mm diameter electron beam, up to temperatures within the 175–360°C range; most of the irradiations were performed at 290°C. In order to allow electrical resistivity measurements and to minimise the temperature gradients, the sample was held by four 0.1 mm diameter chromel wires welded on its corners on one end and fixed to two copper rods on the other end; the chamber was filled with 0.7 atm Helium gas. The voltage is measured by way of two wires welded symmetrically at 0.5 cm from the center. Finally a thermocouple (copper/constantan of 100 μm of diameter) was welded onto the sample, on the middle of the top edge. With this geometry, a calculation (validated by a good agreement with the temperatures measured by three thermocouples) shows that, for a central temperature of 290°C, the temperature difference between the center and a point at 0.5 cm do not exceed 5°C.

2.4. Electrical resistivity measurements

Due to its huge sensitivity, the electrical resistivity technique is used to follow 'in line' the early stages of precipitation. In order to decrease the phonon component, it is not measured at the irradiation temperature, but at 30°C. With this aim in view, the electron beam is shut down periodically. The temperature of 30°C is reached in less than two minutes. The electrical resistance is measured by the classical direct current (dc) four points method. Two measurements are performed, reversing the dc direction and the average value is taken. Between the two measurements, triggered automatically by computer assistance, the temperature decreases by less than 1°C.

With our sample geometry, one difficulty is to get the form factor (for the resistivity measurement). An initial experiment with an optimised geometry allowed to calibrate the resistivity of the material before irradiation, therefore giving a true value of the actual form factor. Furthermore this calibration experiment showed that the electrical resistivity of our *Fe*Cu alloys in the homogeneous (solid solution) state increases linearly, at a given T, with copper content. At 30°C it is given by the equation:

$$\rho_{FeCu}(\mu\Omega\ \text{cm}) = \rho_{Fe} + 3.9(\pm 0.4)[\text{Cu}]_m. \quad (1)$$

Here $[\text{Cu}]_m$ is the matrix copper content in atomic percent and $\rho_{Fe} = 10.4 \pm 0.4$ μΩ cm is the resistivity (at 30°C) of pure iron.

If we suppose that the precipitate contribution can be neglected, the resistivity change is directly related to the matrix solute depletion during aging. This assumption will be discussed in detail in Section 3.1.1.

In order to compare in a simple way the kinetics of copper depletion in the matrix for various materials and environmental variables, let us define a simple parameter that we shall call the precipitation kinetics parameter $F_{1/4}$ as the reciprocal of the time needed to reach an advancement factor $\xi = \frac{1}{4}$. The advancement factor is $\xi = ([\text{Cu}]_{m,i} - [\text{Cu}]_{m,t})/([\text{Cu}]_{m,i} - [\text{Cu}]_{m,\infty})$ where $[\text{Cu}]_{m,i}$, $[\text{Cu}]_{m,t}$ and $[\text{Cu}]_{m,\infty}$ are, respectively, the copper concentrations in the matrix at the beginning, at time t and at the end of the precipitation process. If the precipitate contribution to the resistivity is neglected, we have $\xi = \backslash F(\rho_i - \rho(t); \rho_i - \rho_\infty)$ where ρ_i, $\rho(t)$ and ρ_∞ are, respectively, the electrical resistivity of the sample at the beginning of precipitation, at time t and at a time long enough for the resistivity not to vary significantly any longer.

2.5. Small angle neutron scattering (SANS)

The SANS experiments were carried out at the Laboratoire Léon Brillouin (CEA-CNRS), CEA Saclay, on the PAXY and PAXE spectrometers, at room temperature under saturating magnetic field $H = 1.4$ T perpendicular to the neutron beam direction. The total width at half maximum of the wavelength distribution is $\cong$ 10% of the nominal 0.6 nm wavelength. The two-dimensional position sensitive detector was placed at a distance of 3.28 m from the sample, covering a scattering vector $\vec{q}$ from 0.1 to 1.2 nm^{-1}.

Let us describe with some details our procedure in order to point out that the SANS technique, currently used for aging studies under irradiation, is not as straightforward as often believed, especially concerning the interpretation of the so-called A ratio for small precipitate radius, to be defined later.

We assume that during aging, a distribution $h(R)$ of

spherical precipitates of radius R appears. In a first step, we also assume that the chemical composition and the magnetisation are homogeneous in the ferritic matrix as well as in the precipitate.

After normalisation and subtraction of the intensity scattered by a reference sample (with the same composition and microstructure than the studied sample but not thermally aged or irradiated) and assuming that the precipitates are randomly distributed, the SANS intensity per unit volume is given by

$$\frac{1}{V_s}\frac{d\Sigma}{d\Omega}(q) = f_p\left(\Delta\rho_{nucl}^2 + \Delta\rho_{mag}^2 \sin^2\alpha\right) \times \frac{\int_0^\infty h(R)V^2(R)F^2(q,R)\,dR}{\int_0^\infty h(R)V(R)\,dR}, \quad (2)$$

where V_s is the sample irradiated volume, f_p is the volume fraction of precipitates, α is the angle between the scattering vector and the magnetisation of the sample, q is the magnitude of the scattering vector, $V(R)$ is the volume of a spherical particle of radius R, $F(q, R) = 3((\sin qR - qR\cos qR)/(qR)^3)$ is the form factor of a spherical particle,

$$\Delta\rho_{nucl} = \frac{b_{nucl}^p}{v_a^p} - \frac{b_{nucl}^m}{v_a^m} \quad (3)$$

is the nuclear contrast. Here $b_{nucl}^{m,p}$ and $v_a^{m,p}$ are the nuclear scattering length and the atomic volume for the matrix (m) and precipitate (p). We used the scattering length values given recently by Sears [9]: $b_{Fe} = 0.945 \times 10^{-12}$ cm and $b_{Cu} = 0.7718 \times 10^{-1}2$ cm. $\Delta\rho_{mag}$ is the magnetic contrast. In our alloys, as only iron atoms induce magnetic scattering, and assuming pure copper precipitates, $\Delta\rho_{mag}$ is given by

$$\Delta\rho_{mag} = \frac{-b_{mag}^m}{v_a^m} = -\frac{\gamma r_o}{2v_a^m}\mu_{Fe}, \quad (4)$$

where $\gamma = -1.913$ is the gyromagnetic factor of the neutron, $r_o = 0.2818 \times 10^{-14}$ m is the classical electron radius and μ_{Fe} is the magnetic moment of iron atom.

Eq. (2) was used to fit the experimental data. The factor $f_p\ (\Delta\rho_{nucl}^2 + \Delta\rho_{mag}^2)\sin^2\alpha$ as a whole was considered as a fitting parameter.

2.5.1. The size distribution of the precipitates

Four precipitate radius distributions $h(R)$ were tested. Two are empirical and have two fitting parameters: The symmetric normalised on [0, $+\infty$] Gaussian distribution and the non-symmetric log–normal distribution. Two are given by the Lifshitz–Slyosov–Wagner coarsening theory (LSW) depending on the growth kinetic model considered. They have only one fitting parameter [10]. The first one (LSW1), strongly asymmetric applies, when the coarsening is diffusion controlled and the second one (LSW2), less asymmetric, applies when the coarsening is interface-reaction controlled.

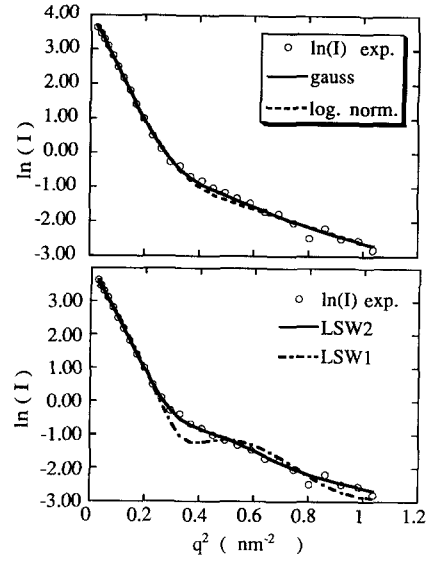

Fig. 1. Fit of the SANS intensity profile of the $FeCu_{1.34\ at\%}$ aged 142 h at 500°C with different size distributions of precipitates; LSW1 ($R_m = 6.8$ nm), LSW2 ($R_m = 6.6$ nm), Log–normal ($R_m = 7.0$ nm and $\Delta R = 1.5$ nm)) and Gaussian ($R_m = 6.3$ nm and $\Delta R = 2$ nm)).

In order to know the importance of the error induced by the neutron wavelength distribution, the scattered intensity profiles were fitted either taking or not taking it into account.

For shortly aged samples, the scattered intensity profile is linear in a Guinier's plot (ln I versus q^2) within the q studied range ($q < 1.2$ nm^{-1}) and the fits are good whatever the size distribution of precipitates. The mean radius depends weakly on the radius distribution and no information can be obtained on the shape $h(R)$ of the distribution.

For samples thermally aged for long times or irradiated at high doses, the neutron scattering intensity is no more linear in Guinier's representation within the whole studied q range (Fig. 1). The Gaussian and LSW2 distributions give the best fits. The log–normal is not so good and the LSW1 very bad. By taking into account the wavelength distribution, the fits remain good for the Gaussian and LSW2 distributions but, in the case of the LSW1 distribution, even if the scattered intensity oscillations are reduced, the fit is unacceptable.

We decided to use the gaussian distribution, on the one hand because it has two fitting parameters, but also because the precipitate size distributions observed experimentally by transmission electron microscopy are usually more symmetrical that those given by LSW theories [11]. This distribution is given by

$$h(R) = \frac{1}{\sqrt{2\pi}\sigma}\exp\left[-\frac{(R-R_m)^2}{2\sigma^2}\right], \quad (5)$$

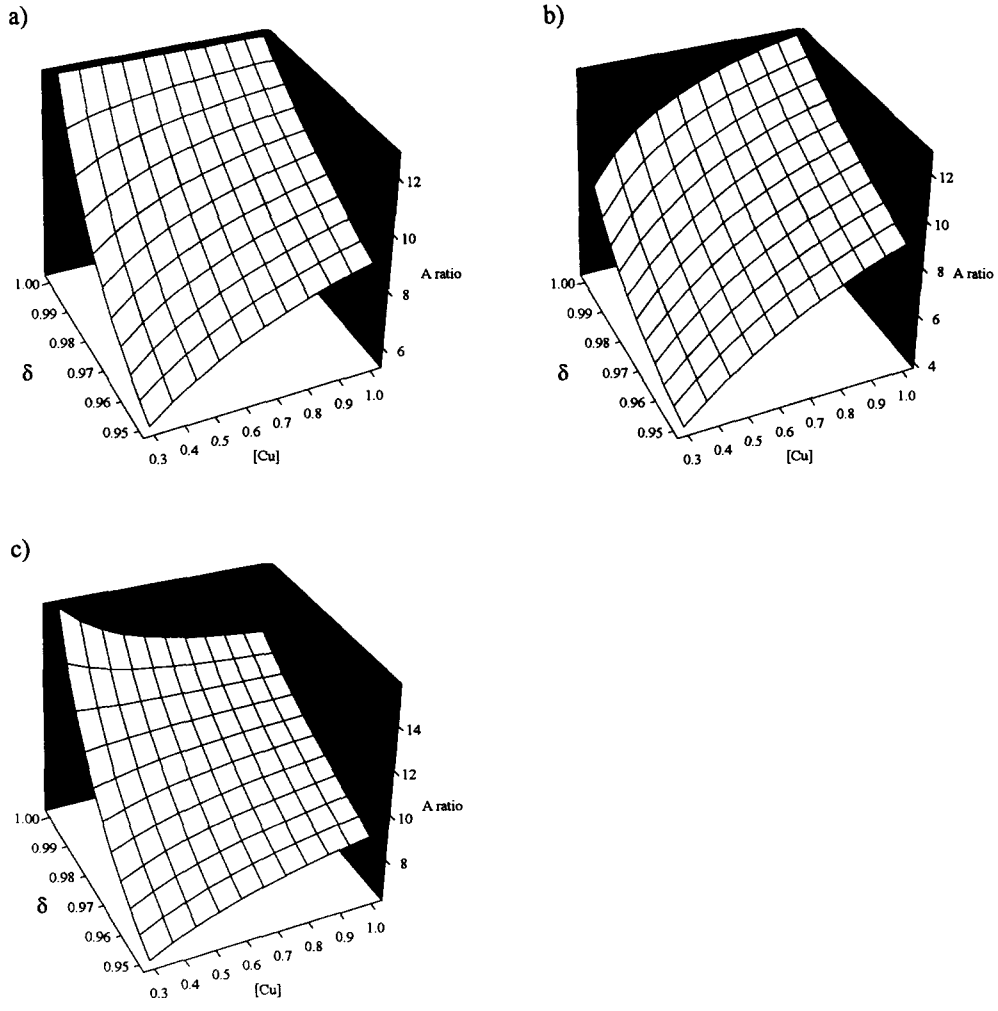

Fig. 2. Effect on the A ratio of the copper concentration and of the atomic volume for various magnetic moment per iron atom in the precipitate normalised to the magnetic moment per iron atom in pure iron ($\hat{\mu}$): (a) $\hat{\mu} = 1$; (b) $\hat{\mu} = 1.1$ and (c) $\hat{\mu} = 0.95$.

where R_m is the mean radius. The half-width of the size distribution at half maximum ΔR is given by $\Delta R = \sqrt{2 \ln 2}\,\sigma = 1{,}177\sigma$.

2.5.2. About the A ratio

In order to determine the precipitated volume fraction and the number density of clusters, we have to know the contrast or in other words the precipitate chemical composition. The so-called A factor contains some information about this chemical composition. The A factor is defined as the ratio between scattered intensifies measured perpendicular and parallel to the sample magnetisation. For chemically and magnetically homogeneous particles, it is then given by

$$A = \left(\frac{d\Sigma}{d\Omega}\right)_{\perp \vec{H}} \Bigg/ \left(\frac{d\Sigma}{d\Omega}\right)_{//\vec{H}} = 1 + \left(\frac{\Delta\rho_{mag}}{\Delta\rho_{nucl}}\right)^2$$

With the simplest assumption, i.e., for pure copper particles with the same atomic volume than in the surrounding matrix, we find $A = 12.92$. As this value is significantly higher than the measured ones, we studied the influence of some relevant parameters in order to discuss the origin of this apparent discrepancy.

The A value may a priori depend on the ratio of the atomic volumes in the precipitate and in the matrix, noted $\delta = v_a^m / v_a^p$, on the copper concentration in the precipitate $[Cu]_p$ and on the magnetic moment per iron atom in the precipitate, when the iron content in the precipitate is high enough to get ferromagnetic precipitates. The A ratio is then given by

$$A = 1 + \left[\frac{b_{mag}^{Fe}\left[\left(1 - [Cu]_p\right)\hat{\mu}\delta - 1\right]}{[Cu]_p\,\delta\left[b_{Cu} - b_{Fe}\right] - b_{Fe}(1-\delta)}\right]^2, \qquad (6)$$

where $\hat{\mu}$ is the ratio of the magnetic moment per iron atom

in the precipitate and in the matrix (it seems that in the *Fe*Cu system it can be larger than 1 [12]).

Let us first consider the effect of the atomic volume in the precipitate for pure copper precipitates ($[Cu]_p = 1$, $\hat{\mu} = 0$): A decreases significantly when δ decreases (Fig. 2a). The effect of $[Cu]_p$ is much more complicated. It is often claimed that with $\delta = 1$, $[Cu]_p$ has no effect on A. This conclusion is wrong, because it stands on the non-physical implicit assumption that $\hat{\mu} = 1$ whatever the Cu concentration. In fact $\hat{\mu}$ is close to 1 if the precipitate is ferromagnetic, but must be equal to zero in other cases. The critical copper concentration below which the precipitate is no longer ferromagnetic at room temperature is unfortunately not known. In the non-ferromagnetic state, A increases with the iron concentration in the precipitate from 12.92 for $[Fe]_p = 0$ up to 19.62 for $[Fe]_p = 0.2$. The behaviour of A for precipitates in the ferromagnetic state is given on Fig. 2. It appears that if A does not change with $[Cu]_p$ for $\delta = 1$ and $\hat{\mu} = 1$, this is no more true when $\hat{\mu} \neq 1$.

In conclusion, the value of the A ratio for homogeneous precipitates depends strongly on the $[Cu]_p$, δ and $\hat{\mu}$ values.

Until now we considered the case of an homogeneous precipitate with a sharp precipitate–matrix interface. Let us now study the case of a non-homogeneous precipitate. We have considered a simplified model: a pure copper core surrounded by a shell containing copper and iron. The form factor of this kind of particle can be approximated by two concentric spheres. The A ratio is then given by

$$A = 1 + \Big[\Big(\big(\Delta\rho_{mag1} - \Delta\rho_{mag2}\big) R_1^3 F(q, R_1) + \Delta\rho_{mag2} R_2^3 F(q, R_2)\Big) \Big/ \Big(\big(\Delta\rho_{nucl1} - \Delta\rho_{nucl2}\big) R_1^3 F(q, R_1) + \Delta\rho_{nucl2} R_2^3 F(q, R_2)\Big)\Big]^2, \quad (7)$$

where R_1 and R_2 are the radius of the core and the radius of the core plus the shell, respectively, $\Delta\rho_{nucl1}$ and $\Delta\rho_{mag1}$ are the nuclear and the magnetic contrast between pure copper core and the matrix (given by Eqs. (3) and (4)), $\Delta\rho_{nucl2}$ and $\Delta\rho_{mag2}$ those between the shell and the matrix. Eq. (7) depends on the copper content [Cu], on the thickness $(R_2 - R_1)$ of the shell and on the parameters δ and $\hat{\mu}$ introduced previously. For instance, with the parameters $[Cu]_{shell} = 0.5$, $\delta = 0.95$ and $\hat{\mu} = 1.05$, we found for a given value of the shell thickness, that the A value depends on q (weakly at small and medium q and strongly at large q). Furthermore, the A ratio for a given value of R_2 depends strongly on R_1 for small R_1 values and saturates at high precipitate radius ($R_1 \to R_2$) at the expected value for homogeneous precipitates [13].

3. Results

As the main part of our results concerns the 1.34 at.% copper alloy, those concerning lower concentrations will be only given at the end of the paragraph.

3.1. Electron irradiation at 290°C and thermal aging at 500°C

3.1.1. Electrical resistivity

The electrical resistivity versus fluence dependence of the $FeCu_{1.34\%}$ sample irradiated at 290°C up to 5 C/cm^2 is plotted in Fig. 3. The resistivity decreases very rapidly from 15.5 to 11.7 $\mu\Omega$ cm at 0.8 C/cm^2 and then more and more slowly down to 11.5 $\mu\Omega$ cm at 5 C/cm^2. In order to know if the use of Eq. (1) to get the matrix copper content $[Cu]_m$ is correct, i.e., if the precipitate contribution to the resistivity can be neglected, let us compare the $[Cu]_m$ value obtained by using Eq. (1) and the $[Cu]_m$ values obtained by tomographic atom probe (TAP). At 0.15 C/cm^2, Eq. (1) gives $[Cu]_m = 0.80$ at.% and TAP gives $[Cu]_m = 0.70 \pm 0.10$ at.% [14]: the precipitate contribution is negligible at low doses, i.e., when the precipitation is far from being completed.

This is no more true at high doses when the matrix is almost totally depleted. At 5 C/cm^2, Eq. (1) gives $[Cu]_m = 0.30$ at.%. Unfortunately, no TAP experiments were carried out on this sample. However, as at this fluence the precipitation is completed since a long time, $[Cu]_m$ should be equal to the solubility limit of copper in iron C_c at 290°C. Extrapolation from high temperature data (690–840°C) [15], assuming an Arrhenius law, yields $C_c = 2 \times 10^{-4}$ at.%. As such an extrapolation over a large temperature range is highly questionable, the recent value $C_c = 4.0 \times 10^{-2}$ at.% given by Jackson et al. [16] is certainly better. This latter value is not too far from the TAP results: $0.08 < C_c < 0.1$ at.% (no precipitation observed in a $FeCu_{0.08}$ at.% at 290°C and $[Cu]_m = 0.10$ at.% in $FeCu_{0.7\%}$ electron irradiated at 290°C up to 1.1 C/cm^2 (mean radius of the precipitates around 2.5 nm)). The $[Cu]_m$ value deduced from electrical resistivity is hence clearly too

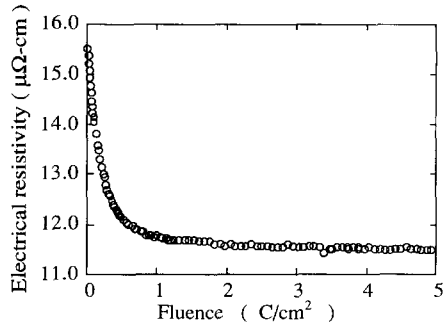

Fig. 3. Electrical resistivity versus fluence of the $FeCu_{1.34\%}$ sample irradiated at 290°C.

high: the precipitate contribution cannot be neglected as soon as the depletion of the matrix is important.

In conclusion:

(a) The behaviour of the electrical resistivity during precipitation in *Fe*Cu alloys is not pathologic such as, for instance, in *Al*Zn [17]. The resistivity per precipitated copper atom is smaller than the one per matrix copper atom whatever the size of the precipitates.

(b) Eq. (1) gives a good estimate at the beginning of precipitation. The precipitation kinetics parameter $F_{1/4}$ used to compare in a simple way the kinetics of copper depletion in the matrix for various materials and environmental variables, is meaningful. Since the fraction of precipitated copper atoms is small, its contribution to the resistivity remains small compared to the contribution of the matrix copper atoms.

(c) The precipitate contribution to the resistivity cannot be neglected when the advancement of the precipitation process is important. The contribution of the precipitated copper atoms is then very large as compared to the contribution of the copper matrix atoms.

3.1.2. Small angle neutron scattering

The mean radius R_m given by SANS (Table 1) increases continuously with aging time in both irradiated and thermally aged samples. The $\Delta R/R_m$ ratio increases rapidly up to a value of 0.35 and then remains approximately constant.

For $R_m > 2$ nm, the measured values of the A ratio are between 8 and 10. These values are significantly smaller than the one calculated by using the recent scattering lengths given by Sears [9] and assuming pure copper non-ferromagnetic precipitates ($A = 12.9$, cf Section 2.5.2). This question has never been raised in the literature because the authors used the old scattering lengths given by Bacon in 1975 [18] (for which one calculates $A = 10.9$). The discrepancy can be overcome by simply assuming that the lattice parameter in the pure bcc copper precipitate (a_p) is slightly higher than in the matrix (a_{Fe}). Calculation gives $A = 10$ for a ratio $a_p/a_{Fe} = \delta^{1/3}$ as small as 1.012. This value is in good agreement with the EXAFS results [6].

Under both irradiation and isothermal aging, the A ratio value is systematically lower for short aging times ($6 < A < 8$). An analysis of the A ratio values published in the literature [19] confirms this behaviour. We think that the relevant parameter is not the aging time or dose but the precipitate radius. The interpretation of this behaviour is complex. Akamatsu [19] for electron as well as Buswell et al. [20] for neutron irradiated samples explain small A values (6–7) by assuming the presence of $\approx 15\%$ iron and $\approx 7\%$ vacancies in the precipitates. However, such an analysis is only valid if the precipitate contains enough iron to be ferromagnetic, has a perfectly spherical shape and a sharp interface with the matrix. The results obtained by tomographic atom probe [14] on our samples irradiated up to 0.15 C/cm^2 at 290°C or thermally aged 2.5 h at 500°C, show pure copper precipitates with ramified interfaces. As the roughness of the interface is of the order of some atomic distances, the effect on the A ratio, if any, will be significant only for small precipitates. The A ratio for such precipitates is difficult to calculate. In order to use the simple model exposed in Section 2.5.2 we replace the irregular interface by a shell in which the copper concentration is equal to 50%. Taking $\hat{\mu} = 1.1$, $a_p/a_{Fe} = 1.012$ and $R_2 - R_1 = 0.5$ nm, we found (in the $q < 1.5$ nm^{-1} range) A equal to 6 and 7 with, respectively, a core radius R_1 equal to 0.5 nm and 1 nm. This result shows that the A ratio values can be explained in terms of interface structure and atomic volume change only without assuming vacancies in the precipitate as it is usually done.

Table 1
Summary of SANS results on $FeCu_{1.34\ at.\%}$ irradiated with 2.5 MeV electrons at 290°C or thermally aged at 500°C

Electron irradiation at 290°C					
Dose (C/cm^2)	R_m (nm)	ΔR (nm)	f_p (%)	A	N_p/cm^3 ($1 \times 10^{+17}$)
0.15	$1.2 \pm .2$	$0.15 \pm 0{,}1$	0.8 ± 0.2	$7.5 \pm .5$	~ 10
0.5	$2.1 \pm .3$	$0.35 \pm 0{,}2$	0.9 ± 0.3		2 ± 1
1.6	$2.5 \pm .3$	$0.8 \pm 0{,}2$	0.9 ± 0.3	$8.3 \pm 1.$	1.2 ± 0.5
1.8	$2.6 \pm .3$	$0.9 \pm 0{,}2$	0.9 ± 0.3	8.4 ± 1.2	1.1 ± 0.5
5	$3.2 \pm .2$	$1.0 \pm 0{,}15$	1.13 ± 0.2	$9.4 \pm .8$	0.66 ± 0.2
Thermal aging at 500°C					
Time (h)	R_m (nm)	ΔR (nm)	f_p (%)	A	N_p/cm^3 ($1 \times 10^{+17}$)
2.5	$0.9 \pm .2$	0.17 ± 0.1	~ 0.7	$6.5 \pm .5$	~ 20
4.5	$2.3 \pm .3$	0.35 ± 0.2	1.1 ± 0.3	$9.3 \pm .3$	1.7 ± 1.1
8	$2.9 \pm .3$	0.9 ± 0.2	1.1 ± 0.3	$9. \pm .4$	0.8 ± 0.5
25	$3.0 \pm .3$	0.9 ± 0.2	0.92 ± 0.3	$9.2 \pm .4$	0.7 ± 0.3
142	$6.3 \pm .3$	2.0 ± 0.4	0.95 ± 0.3	9.4 ± 1	$7 \pm 3 \times 10^{-2}$
312	$8.0 \pm .4$	2.3 ± 0.3	1 ± 0.3	$7.4 \pm .3$	$4 \pm 1 \times 10^{-2}$

For very long thermal aging, the A ratio seems to decrease. This behaviour, only observed in one case (312 h at 500°C), is not explained.

To calculate the number density of clusters N_p given in Table 1, we assumed that the precipitates are pure copper. For the Gaussian size distribution of precipitates used, it is given by

$$N_p = \frac{3}{4\pi} \frac{f_p}{\left(3\sigma^2 + R_m^2\right) R_m} \quad \text{with } \sigma = \Delta R / 1.177.$$

It is worth noticing that our SANS results on the thermally aged samples at 500°C are in good agreement with the Kampmann and Wagner values [21] at the same temperature.

As summary, Fig. 4 shows (a) the matrix copper concentration calculated from the electrical resistivity without taking into account the precipitate component to the electrical resistivity (cf. Section 3.1.1), (b) the radius and (c) the number density of precipitates versus fluence under irradiation at 290°C or aging time during thermal treatment at 500°C. Irradiation and thermal aging behaviours are identical by standing the following scaling law: *1 C/cm² at 290°C under electron irradiation corresponds to 9 h under thermal aging at 500°C*. Furthermore, the incubation time (if any) is very short and N_p decreases since the early stages: the coarsening starts before the total depletion of the matrix. This latter point is confirmed by the fact that a log–log plot of R_m versus time shows a $t^{1/3}$ law under irradiation as well as during thermal aging over the whole aging times (or doses) range (Fig. 5).

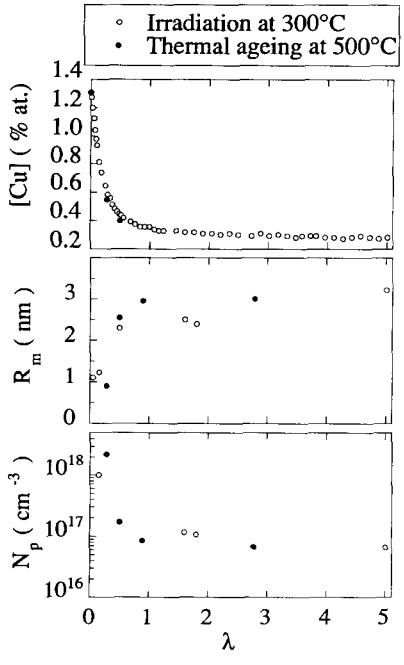

Fig. 4. Evidence of a scaling law for $FeCu_{1.34\%}$. λ is the scaling coefficient defined as $\lambda = 1$ C/cm² at 290°C under electron irradiation or 9 h under thermal aging at 500°C.

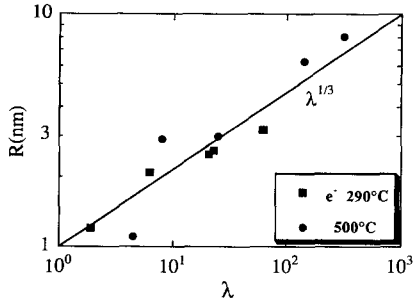

Fig. 5. Log–log plot of the mean radius of the precipitates versus time or electron fluence for the $FeCu_{1.34\%}$ alloy thermally aged at 500°C or irradiated at 290°C.

3.2. Effect of the irradiation temperature

The same alloy was irradiated at various temperatures in the range 175–360°C. As shown previously at a higher flux [4], the electrical resistivity decreases the more slowly the lower the temperature (Fig. 6): the precipitation kinetics parameter $F_{1/4}$ increases with the irradiation temperature. Compared to its value at 290°C, it is 7.5 times larger at 360°C and only 3.7 and 6 times smaller at 215 and 175°C, respectively. As for the highest flux [1], ξ follows approximately a Mehl–Avrami law with a surprisingly low time (or fluence) exponent ranging from 0.67 at 360°C to 1.4 at 175°C.

The mean radius determined by SANS at 0.5 C/cm² (Table 2) increases with the irradiation temperature and the number density decreases. Furthermore, the A ratio has the same behaviour as discussed before: it is weak (6–7) for the lowest irradiation temperatures (175–215°C) when the mean radius is around 1 nm and high (8–10) when the radius is larger than 2 nm.

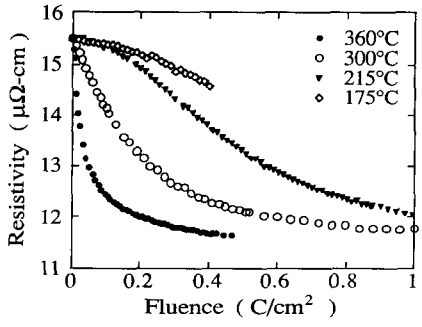

Fig. 6. Effect of the irradiation temperature on the resistivity versus fluence curve for $FeCu_{1.34\%}$.

Table 2
SANS results on $FeCu_{1.34\ at.\%}$ irradiated up to 0.5/cm^2 at various temperatures

T (°C)	R_m (nm)	ΔR (nm)	A	f_p (%)	N_p/cm^3 (1×10^{17})
175	1.0±0.2	0.1±0.1	6.2±0.9	1.6±0.3	40±30
215	1.2±0.2	0.2±0.1	6.5±0.5	1.4±0.2	14±10
300	2.1±0.3	0.35±0.2	10.2±0.5	0.9±0.3	2.0±1.0
360	2.3±0.3	0.5±0.2	8.2±1.4	0.8±0.2	1.3±1.1

3.3. Flux effect

Comparison of the electrical resistivity results with those previously published at a larger electron flux shows that the precipitation kinetics is 2.1 times faster for a flux 4 times larger (Fig. 7). This is consistent with a recombination regime for the elimination of point defects, which gives a flux$^{1/2}$ law.

3.4. Dislocation density effect

Two states of the $FeCu_{1.34\%}$ alloy with different dislocation densities were irradiated at 290°C. The first one was the standard 'annealed–quenched' state (AQ) with a low dislocation density ($\rho_d \cong 10^8$ cm^{-2}) and the second one was simply the cold-rolled state (CR) obtained just before annealing. In the later state, the dislocation density cannot be measured by transmission electron microscopy but is supposed to be around 10^{11} cm^{-2}. Fig. 8 shows that the resistivity changes more slowly in the CR sample. The precipitation kinetics parameter $F_{1/4}$ is 1.7 times smaller than in the AQ sample.

SANS characterisation after irradiation up to 0.5 C/cm^2 has also been carried out. If, as already shown in Section 2.5.1, the $I(q)$ curve can be fitted with only one gaussian distribution for the AQ sample, for the CR one, it is necessary to introduce two Gaussian distributions. Table 3 shows that the first one gives the same parameters as the one obtained in the AQ sample and that the second one gives a mean radius two times larger and a volume fraction 20 times smaller. Though we did not perform electron microscopy observations on this sample, we think that the second distribution may correspond to precipitation on dislocations.

It is difficult to infer from these results if the effect of the dislocation density on the precipitation kinetics comes from the existence of the second population of precipitates which nucleates early on the dislocations or because, as it is well known for high dislocation density, the point defects are preferentially eliminated on dislocations with the consequence that, contrarily to what happens in the recombination regime, the diffusion coefficient depends on the dislocation density.

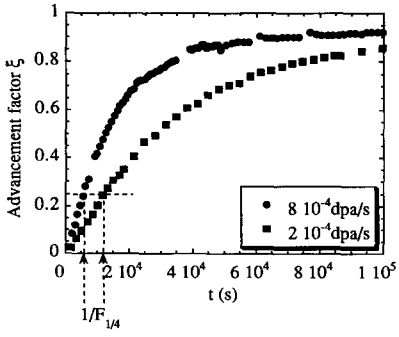

Fig. 7. Flux effect on the advancement factor ξ versus time curve for $FeCu_{1.34\%}$ irradiated at 290°C.

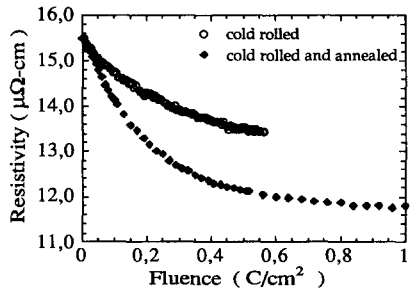

Fig. 8. Effect of the dislocation density on the resistivity versus fluence curve for $FeCu_{1.34\%}$ irradiated at 290°C.

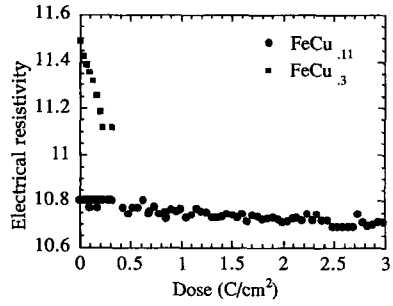

Fig. 9. Resistivity versus fluence for $FeCu_{0.30\%}$ and $FeCu_{0.11\%}$ irradiated at 290°C.

Table 3
SANS results obtained on cold rolled (CR) or annealed (AQ) $FeCu_{1.34\ at.\%}$ samples electron irradiated at 290°C at a fluence of 0.5 C/cm^2

State		R_m (nm)	ΔR (nm)	f_p (%)	N_p/cm^3 (1×10^{17})
CR	1st distribution	2.0±0.2	0.6±0.1	0.7	2±1
	2d distribution	4.2	1.9	0.031	7×10^{-3}
AQ		2.1±0.3	0.35±0.2	0.9	2±1

Table 4
Summary of SANS results on $Fe Cu_{0.3\ at.\%}$ electron irradiated at 290°C

Dose (C/cm^2)	R_m (nm)	ΔR (nm)	N_p/cm^3 (1×10^{17})	f_p (%)	A
0.5	1.1	0.5	0.9	0.09	5.5 ± 2
1.5	1.30	0.45	1.65	0.2	5 ± 2
2.5	1.44	0.5	1.42	0.25	5 ± 1

3.5. Copper concentration effect

Aging under irradiation was studied as a function of the fluence in the 0.30 and 0.11 at.% Cu alloys at 290°C only.

A significant decrease of the electrical resistivity appears in both alloys (Fig. 9). Compared with the 1.34 at.% Cu alloy, the precipitation kinetics parameters are 6 and 28 times smaller, respectively, in the 0.30 and 0.11 at.% alloys. In the 0.11 at.% alloy irradiated up to 5 C/cm^2, the electrical resistivity gives $[Cu]_m \leq 0.09$ at.%.

SANS measurements in the 0.30% alloy yield a mean radius at 1.5 C/cm^2 which is approximately two times smaller and a number density which is the same than in the 1.34% Cu alloy (Table 4). At 2.5 C/cm^2, R_m is only equal to 1.44 nm. Here again we observe a small A ratio ($\cong 5$) for small precipitate radius.

On the other hand, no significant SANS signal is observed in the 0.11% copper alloy. This fact can be explained by the very low volume fraction of probably very small precipitates.

As tomographic atom probe did not show any precipitation in a 0.08 at.% Cu alloy irradiated at 290°C up to 2×10^{19} e^-/cm^2 [22], one can infer that the copper precipitation limit at 290°C is located between 0.09 and 0.08 at.% Cu. Surprisingly, even in the lowest copper content alloy, no incubation time for precipitation is observed. If it would exist, electrical resistivity measurement would be able to detect it.

4. Discussion and modelling

In this fourth part, we discuss the limitations of the existing models for copper precipitation under irradiation and present a new one. We also carry out a comparison between. the results obtained under electron and neutron irradiations.

4.1. Modelling of copper precipitation

In the early model proposed by Odette et al. [23], it was assumed that the only effect of neutron irradiation is to enhance the diffusion coefficient of copper and that the nucleation is so fast that small precipitates are immediately present at the beginning of irradiation (at a number density which is a parameter of the model). A criticism which could be raised is that this model does not take into account the coarsening which, as shown in the present work, is clearly involved in the $Fe Cu_{1.34\ at.\%}$ alloys, at least when the mean radius of the precipitates is larger than 1.0 nm. However, as shown in Table 4 (where NpH does not decrease with increasing dose for $Fe Cu_{0.3\ at.\%}$), this criticism is probably not relevant for lower copper content ($\leq 0.3\%$ up to 2.5 C cm^{-2}). The assumption that the effect of electron irradiation is to simply enhance the precipitation kinetics and not to promote a new mechanism of precipitation (such as the one which is at the origin of the so called radiation-induced precipitation in undersaturated solid solutions [24,25]), is highly sustained by our work for the case of electron irradiation: on the one hand, by the similarity of the resistivity as well as the precipitate radius and number density versus time curves under irradiation and thermal aging at higher temperature (see Fig. 5) and on the other hand by the similar microstructure of precipitates observed by high resolution electron microscopy for long irradiation or thermal aging time [26]. Nevertheless we shall see below, Section 4.2, that this model does not apply to neutron irradiation.

More recently, the Langer and Schwartz (LS) model [27] was extended to an irradiation situation to fit the electrical resistivity measurements carried out by Le et al. [4]. It was shown that for the $Fe Cu_{1.34\ at.\%}$ alloy under electron irradiation in the 175–370°C range as well as under thermal aging in the 390–490°C range, a fit is only possible by assuming that the precipitates are present at the beginning with a number density N_{pb} independent on the temperature [28]. However, taking a reasonable value for the precipitate interfacial energy, this model gives a too low coarsening rate. This fact was previously observed for thermal aging at 500°C [21]. In order to check whether the hypothesis that the nucleation flux and the coarsening rate of Langer and Schwartz are at the origin of the too low coarsening rate and of the necessity to assume a heterogeneous nucleation, we calculated numerically the precipitation using a cluster dynamics type model which stands on less restrictive hypothesis.

This model assumes spherical pure copper clusters characterised each by only one parameter: the number n of copper atoms within the precipitate. The clusters may grow or shrink by absorbing or emitting a single atom. The master equations describing the change with time of the number density of precipitates C_n containing n atoms is given by

$$\frac{dC_n}{dt} = \beta(n-1)C_{n-1} + \alpha(n+1)C_{n+1} - [\beta(n)+\alpha(n)]C_n \quad \text{for } n \geq 2,$$

$$\frac{dC_1}{dt} = \sum_{n=2}^{\infty} \alpha(n)C_n - \sum_{n=2}^{\infty} \beta(n)C_n - 2\beta(1)C_1 + \alpha(2)C_2 \quad \text{for } n=1. \tag{8}$$

They are nothing but the equations on which are based the Becker and Döring nucleation theory [29]. Eq. (8) was generalised by Binder [30] to allow growth and shrinking not only by evaporation or condensation of monomers but also by small clusters. For dilute alloys as the ones studied in this work, such a complication is certainly not relevant. The impingement rate $\beta(n)$ and emission rate $\alpha(n)$ are given in Appendix A. They are calculated within the framework of the capillary model and the assumption that the detailed balance holds between the growth process and the inverse shrinking process. They only depend on the solubility limit C_e and the interfacial energy σ. The solubility limit is given by experiments [15,16] or by extrapolation for low temperatures. To calculate the interfacial energy, we used an adapted form of the Cahn and Hilliard theory [31]. This model presents the advantage to give a temperature dependence of σ. It depends on two parameters: S^{nc} and Ω which are respectively the non-configurational entropy and the segregation energy of the solution. They are obtained by fitting $C_e(T)$ with

$$C_e = \exp\frac{S^{nc}}{k_B}\exp\left(-\frac{\Omega}{k_B T}\right).$$

The Runge Kutta algorithm was used to solve the set of differential Eq. (8) with a maximum value of n equal to 20 000. Calculations were only performed for the $Fe\mathrm{Cu}_{1.34}$ at.% alloy at 500 and 300°C.

In fact, as the extrapolation of C_e at low temperature is unsafe, we used three (S^{nc}, Ω) couples with the constraint that each set gives approximately the C_e experimental values at high temperature. The three couples and the relevant values of C_e and σ at 500 and 300°C are given in Table 5. The first and third lines of this table correspond approximately to the C_e values given by Refs. [15,16], respectively.

We found that at 500°C:

(a) The calculated precipitate size distribution at 500°C for $Dt = 2.5 \times 10^{-11}$ cm^2 is clearly broader and more symmetrical than the LSW1 distribution with the same most probable precipitate radius, but less symmetrical than a Gaussian distribution (Fig. 10).

(b) As in the LS model, the time dependence of R_m, N_p and $[Cu]_m = C_1$ for the three sets of (S^{nc}, Ω), the three stages (nucleation, growth and coarsening) are clearly separated (Fig. 11). The Dt value at which each stage

Table 5
Parameters used to calculate the copper precipitation

Ω/k (K)	S^{nc}/k	500°C		300°C	
		C_e (at.%)	σ (J/m^2)	C_e (at.%)	σ (J/m^2)
9020	4	5×10^{-2}	0.38	8×10^{-4}	0.5
7910	3	7×10^{-2}	0.35	2×10^{-3}	0.45
6800	2	0.1	0.32	5×10^{-3}	2.4

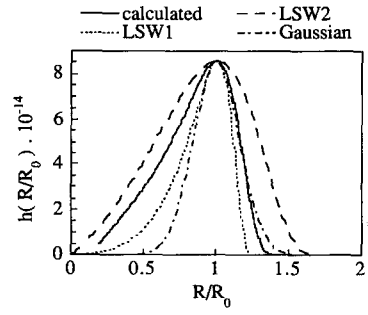

Fig. 10. Calculated size distribution of precipitates for $FeCu_{1.34\%}$ thermally aged at 500°C for $D_t = 2.5\times10^{-11}$ cm^2 ($\Omega/k = 9020$ K). Comparison with Gaussian, LSW1 and LSW2 distributions with the same most probable value R_0.

starts decreases and the maximum number density of precipitates N_{pmax} increases when Ω increases. Fig. 12 gives Np calculated with both models. The incubation time is smaller with the cluster model, the maximum number density of the precipitate and the coarsening rate larger.

(c) Nevertheless, the coarsening rate remain to slow to have the possibility to fit both the nucleation-growth and the coarsening regime (Fig. 13) with the same parameters. An increase by a factor of two and even more of the precipitate-matrix interface energy at the precipitate radius (4 nm) at which the precipitate becomes incoherent, as

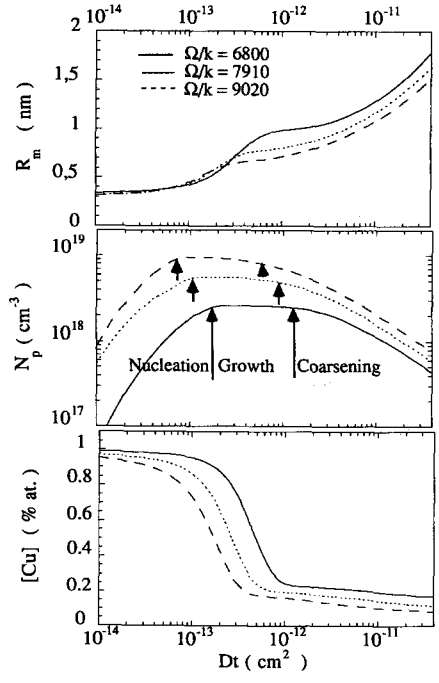

Fig. 11. Change of R_m, N_p and $[Cu]_m$ calculated at 500°C in $FeCu_{1.34\%}$ for the three sets of parameters; (————) Ω/k = 6800 K; (---) Ω/k = 7910 K; (— — —) Ω/k = 9020 K.

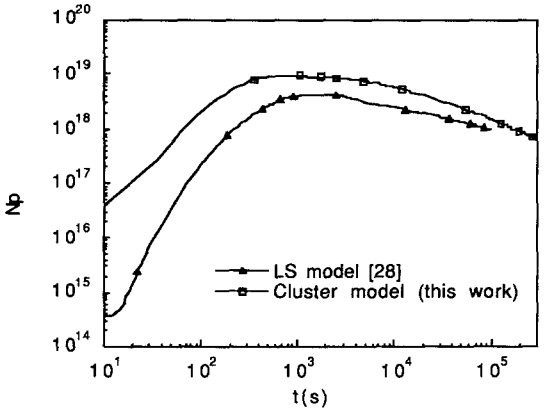

Fig. 12. Number density N_p of precipitates calculated at 500°C with the LS and the cluster models with the same parameters ($\Omega/k = 9020$ K).

suggested by Kampmann et al. [21], does not give any improvement. This difficulty comes clearly from the fact that, on one hand the experiments give for R_m an early $t^{1/3}$ law (before the total solute depletion of the matrix (see Figs. 4 and 5)) but, on the other hand and in agreement with the LSW theory of coarsening, the model gives a $t^{1/3}$ law not for R_m but for $R_m - R_0$ (where R_0 is the precipitate mean radius at the end of the growth stage, when the matrix is totally depleted and below which the behaviour is in $t^{1/2}$).

A possibility to get some improvement is to assume that the reaction kinetics at the interface is not infinite. For this purpose, in the expression of $\beta(n)$ and $\alpha(n)$, D has to be replaced by $RKD/(RK + D)$ where R is the precipitate radius and K the transfer velocity at the precipitate–matrix interface. The best fit (Fig. 14) is then obtained with the ($S^{nc}/k = 2$; $\Omega/k = 6800$ K) couple yielding a C_e value in agreement with [16], $D = 4.0 \times 10^{-15}$ cm^2/s, in agreement with diffusion data and $K = 1.5 \times 10^{-8}$ cm/s. This K value is ten times smaller than the normal transfer velocity in the matrix. The physical origin of such a low transfer velocity at the interface remains unclear.

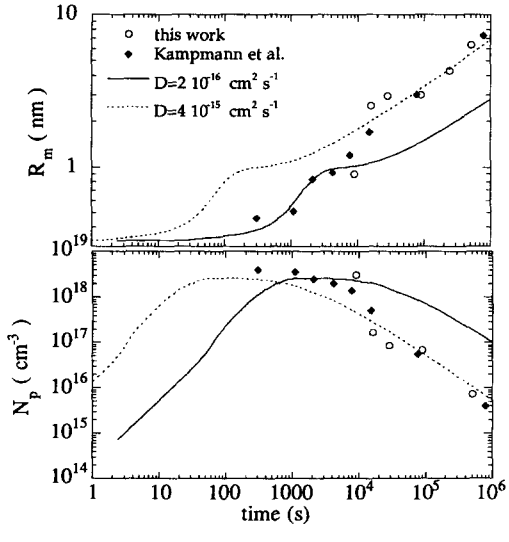

Fig. 13. Mean radius R_m and number density N_p of precipitates calculated for $\Omega/k = 6800$ K and two values of the diffusion coefficient of copper in iron; comparison with experimental data.

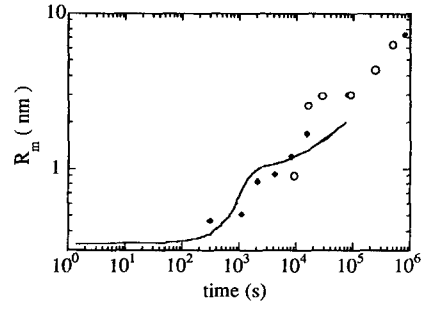

Fig. 14. Calculated mean radius of precipitates versus time in $FeCu_{1.34\%}$ assuming a low transfer velocity, K, at the precipitate-matrix interface ($T = 500$°C, $\Omega/k = 6800$ K, $K = 1.5 \times 10^{-8}$ cm/s, $D = 4.0 \times 10^{-15}$ cm^2/s).

On the other hand, the calculations carried out at 300°C give, whatever the (S^{nc}, Ω) couple, N_{pmax} and even N_p at the end of the growth step (at Dt^* when [Cu] does not change any more quickly) greater than 10^{19} cm^{-3} (Fig. 15). Consequently, as by using the simplest Langer and

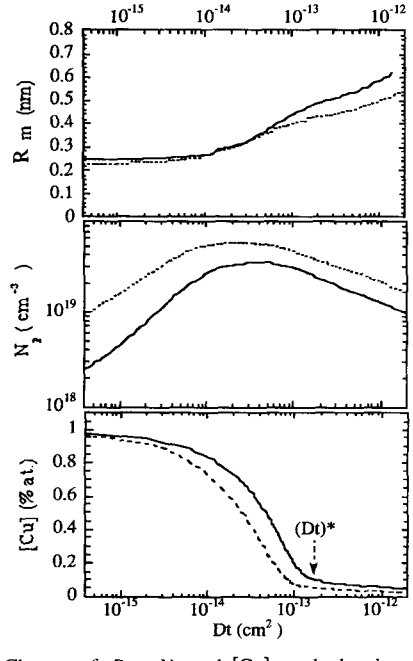

Fig. 15. Change of R_m, N_p and $[Cu]_m$ calculated at 300°C in $FeCu_{1.34\%}$ for: (————) $\Omega/k = 6800$ K and (---) $\Omega/k = 7910$ K.

Schwartz model and whatever the D value and at contrary to the above case of thermal aging at 500°C, we found that it is impossible to fit the experiment under irradiation at 300°C, when an homogeneous nucleation is assumed.

With this cluster dynamics model, it is possible to test the suggestion that the precipitates present at the beginning of irradiation [28] are small supercritical copper clusters appearing during the quench. We found that with a reasonable quenching rate around 10°C/s, this assumption is not valid since nucleation is not suppressed (N_{pmax} is only slightly decreased during a subsequent treatment at 300°C). Since the precipitates are not on dislocations or grain boundaries (at least in the annealed samples) [4], a reasonable hypothesis could be the occurrence of heterogeneous nucleation on impurities. Furthermore, to explain that the number density for a given alloy is independent of temperature [28], it might be assumed that the relevant impurities are saturated. This is probably akin to the fact that no incubation time for precipitation is observed even in the alloy with a copper concentration (0.11 at.%) very close to the copper precipitation limit at 300°C (cf. Section 3.5). However, with such an assumption, the difficulty encountered about the early $t^{1/3}$ behaviour remains if we do not introduce the previously discussed interface precipitate–matrix reaction component.

First results obtained by using a very recent modelling based on a Monte-Carlo simulation on a rigid lattice [32], which has however the inconvenient to permit calculation only up to small precipitate size and which does not consider the non configurational entropy term, seems to overcome the problem about the early $t^{1/3}$ behaviour. It will not be discussed here.

4.2. Comparison of electron and neutron irradiations

For such a comparison, SANS results on neutron irradiated *Fe*Cu at various fluences must be available. The only published results are about an alloy with 1.14 at.% Cu irradiated at two fluences, 1.5×10^{19} and 6.9×10^{19} n cm^{-2} ($E > 1$ MeV) [20]. In order to compare both kinds of particles, we plot R_m versus the fluences expressed in displacements per atom (dpa) (Fig. 16). The fluences for electrons were calculated by using displacement cross-sections equal to 50 barns [33]. For neutrons we used the usual NRT dpa (10^{18} n cm$^{-2} = 1.5 \times 10^{-3}$ dpa). It appears clearly that the behaviour of R_m is completely different under neutron irradiation and under electron irradiation. In the dpa range where experiments exist, R_m (dpa) follows a dpa$^{1/3}$ law under electron irradiation as mentioned previously, but is constant or varies slowly under neutron irradiation. It would be tempting to say that the ratio of the electron dpa over the neutron dpa for reaching a precipitate radius equal to 2 nm is approximately equal to a few hundreds. However, to sustain such an assertion, it would be necessary to get R_m under neutron irradiation at lower doses in order to know whether:

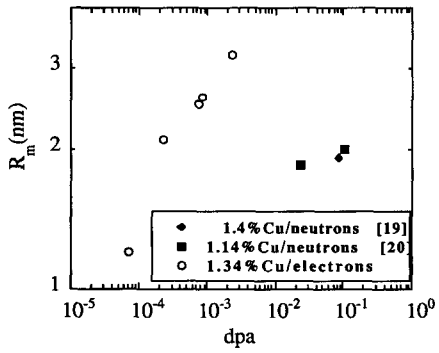

Fig. 16. Experimental values of R_m versus time at 290°C under electron irradiation (this work) and under neutron irradiation in binary *Fe*Cu alloys with 1.1% < [Cu] < 1.4% [19,18].

(i) R_m increases monotonously and saturates near 2 nm or (ii) as observed by SANS in the Chooz pressure vessel steel irradiated under actual conditions [34], the solute clouds radius keep approximately the same value but the number density of clouds increases. Whatever the actual behaviour, the mechanisms of precipitation under electron and neutron irradiation are certainly different. This is in agreement with the results of Pareige et al. [22] which show by tomographic atom probe that precipitates appears in $FeCu_{0.08\ at.\%}$ alloys under neutron irradiation but not under electron irradiation.

5. Conclusion

The development of copper precipitation in binary *Fe*Cu supersaturated solid solutions under electron irradiation which produces only freely migrating defects has been studied with different and complementary techniques: in-situ electrical resistivity for the early stage, SANS under magnetic field for the latter ones. A fine analysis of the effect of several parameters on the so-called A ratio used to get chemical information about the composition of precipitates showed that its interpretation is not as straightforward as usually believed.

The analysis of the experimental results shows that:

(1) At least for the high copper content alloys, the mechanism of precipitation is the same under electron irradiation and thermal aging. In both cases and whatever the copper concentration, the coarsening begins far before the total solute depletion of the matrix and no incubation time is observed.

(2) The kinetics of precipitation increases with the temperature, approximately as the square root of the flux and decreases with increasing dislocation density.

(3) The precipitation limit of copper in iron at 300°C stands around 0.09 at.% Cu.

Furthermore, we developed a new model based on a cluster dynamics approach which gives the precipitate size

distribution for various thermal or irradiation treatments. Even if this model does not overcome all the shortcomings of the previous one based on the Langer and Schwartz method, it nearly fits both SANS and resistivity data if one assumes a low reaction kinetics at the interface and an heterogeneous nucleation.

Finally, the comparison between the changes of the mean radius observed under electron irradiation (this work) and under neutron irradiation (the literature) shows that the corresponding mechanisms of precipitation are very likely different even in alloys with a high concentration of copper.

Acknowledgements

The authors wish to acknowledge Dr P. Vajda for his crucial participation to the calibration of the electrical resistivity of the alloys, Dr F. Boué and Dr A. Brulet for their help in carrying out SANS experiments and J. Ardonceau and G. Jaskierowicz for their technical support.

Appendix A

Modelling the impingement rate $\beta(n)$ is a classical diffusion problem. Assuming that the diffusion field around the spherical cluster do not overlap and that it could not be a perfect absorber, the growth velocity of a precipitate of radius R is given by

$$\frac{\mathrm{d}R}{\mathrm{d}t} = \frac{KD\alpha}{\alpha D + K}(C_\infty - C_R), \tag{9}$$

where C_∞ is the solute concentration at large distance, r_∞, D is the diffusion coefficient, K the transfer velocity through the interface of thickness b, $\alpha = (R+b)/R^2$ and C_R is the solute concentration in equilibrium with a precipitate of radius R. Within the framework of the capillary model, it is given by the classical Thomson–Freundlich equation:

$$C_R = C_e \exp\left(\frac{2\sigma v_a}{k_B T}\frac{1}{R}\right),$$

v_a being the atom volume in the precipitate taken here equal to the atom volume of bcc iron, C_e the solubility limit, σ the interface energy and k_B the Boltzmann constant.

The first term of the right hand side of Eq. (9) may be seen as the growth rate by impingement and the second one as the shrinking rate by emission of solute atoms.

When K is large compared to the transfer velocity in the matrix, given by D/b, the impingement rate is diffusion controlled and is given by

$$\beta(n) = 4\pi\left(\frac{3v_a}{4\pi}\right)^{1/3}(n)^{1/3}DC$$

and the emission rate given $\alpha(n)$ by

$$\alpha(n) = 4\pi\left(\frac{3v_a}{4\pi}\right)^{1/3}(n-1)^{1/3}C_e D \times \exp\left\{\frac{A\sigma}{kT}\left[n^{2/3} - (n-1)^{2/3}\right]\right\},$$

where n is the number of solute atoms contains in a precipitate of radius R_n and $A = (36\pi)^{1/3} v_a^{2/3}$.

As in Ref. [28], the interfacial energy σ is calculated using the Cahn and Hilliard [30] theory adapted for taking into account of a non-configurational entropy term S^{nc}. It is a necessity because the solubility limit of Cu in Fe can be fitted as for a regular dilute solution by $C_e = \exp(S^{nc}/k_B)\exp(-\Omega/k_B T)$ but with $S^{nc} \neq 0$. Then, σ depends on two parameters, S^{nc} and the segregation energy Ω, and is given by

$$\sigma = 1.08\frac{k_B}{a^2}T_c'\left(1 - \frac{T}{T_c'}\right) \quad \text{with } T_c' = \frac{1}{2k_B}(\Omega - TS^{nc}).$$

References

[1] A. Barbu, T.N. Le, N. Lorenzelli, F. Maury, C.H. de Novion, Ann. Chim. Fr. 16 (1991) 352.
[2] F. Maury, N. Lorenzelli, C.H. de Novion, J. Nucl. Mater. 183 (1991) 217.
[3] F. Maury, N. Lorenzelli, C.H. de Novion, P. Lagarde, Scr. Metall. 25 (1991) 1839.
[4] T.N. Lê, A. Barbu, D. Liu, F. Maury, Scr. Metall. Mater. 26 (1992) 771.
[5] M.H. Mathon, F. Maury, A. Barbu, N. Smetniansky, N. Lorenzelli, C.H. de Novion, F. Boué, J. Phys. (Paris) III C3 (4) (1994) 193.
[6] F. Maury, N. Lorenzelli, M.H. Mathon, C.H. de Novion, P. Lagarde, J. Phys.: Condens. Matter 6 (1994) 569.
[7] E. Hombogen, R.C. Glenn, Trans. Metall. Soc. AIME 218 (1960) 1064.
[8] E. Hombogen, H.P. Jung, Z. Metalkd. 55 (1964) 69.
[9] V.F. Sears, Neutrons News 3 (3) (1992) 26.
[10] I.M. Lifshitz, V.V. Slyozov, J. Phys. Chem. Solids 19 (1961) 35.
[11] A.J. Ardell, Acta Metall. 1 (1970) 525.
[12] K. Sumiyama, T. Yoshitake, Y. Nakamura, J. Phys. Soc. Jpn. 9 (1984) 3160.
[13] M.H. Mathon, PhD thesis, University of Paris XI (1995).
[14] P. Pareige, PhD thesis, University of Rouen (1994).
[15] G. Salje, M. Feller-Kniepmeier, J. Appl. Phys. 48 (1977) 1833.
[16] A.J. Kenway-Jackson, J. Mace, R.N. Thomas, W.J. Phythian, Report AEA-RS 4411, 1993.
[17] P. Guyot, J.P. Simon, Scr. Metall. 11 (1977) 751.
[18] G.E. Bacon, Neutron Diffraction, 3rd Ed. (Clarendon, Oxford, 1975).
[19] M. Akamatsu, PhD thesis, University of Paris XI (1994).
[20] J.T. Buswell, C.A. English, M.G. Hetherington, W.J. Phythian, G.D.W. Smith, G.M. Worall, in; Proc. 14th Int. Symp.

on Effects of Radiation in Materials, Vol. 2, Andover, MA, USA, ASTM-STP 1046, 1988, p. 127.
[21] R. Kampmann, R. Wagner, in: Atomic Transport and Defects in Metals by Neutron Scattering, eds. C. Janot, W. Petry, D. Richter and T. Springer, Springer Proc. Phys. 10 (1986) 73.
[22] P. Auger, P. Pareige, M. Akamatsu, J.C. Van Duysen, J. Nucl. Mater. 211 (1994) 194.
[23] G.R. Odette, Scr. Metall. 17 (1983) 1188.
[24] G. Martin, R. Cauvin, A. Barbu, in: Transformations During Irradiation, ed. F. Nolfi (1983) p. 47.
[25] H. Wiedersich, N.Q. Lam, in: Transformations During Irradiation, ed. F. Nolfi (1983) p. 1.
[26] H.A. Hardouin Duparc, R.C. Doole, M.L. Jenkins, A. Barbu, Philos. Mag. 71 (1995) 325.
[27] J.S. Langer, A.J. Schwartz, Phys. Rev. A21 (1980) 948.
[28] N. Smetniansky de Grande, A. Barbu, Radiat. Eff. Def. Solids 132 (1994) 157.
[29] R. Becker, W. Döring, Ann. Phys. Lpz. 24 (1935) 719.
[30] K. Binder, Phys. Rev. B15 (9) (1977) 4425.
[31] J.W. Cahn, J.E. Hilliard, J. Chem. Phys. 28 (1958) 258.
[32] F. Soisson, A. Barbu, G. Martin, Acta Mater. 44 (9) (1996) 3789.
[33] O.S. Oen, Cross-sections for atomic displacements in solids by fast electrons, Report ORNL-4897 (1973).
[34] P. Pareige, J.C. Van Duysen, P. Auger, Appl. Surf. Sci. 67 (1993) 352.